Dual Patterning of Self-Assembling Spider Silk Protein Nanofibrillar Networks

Zan Lamberger, Karolína Kocourková, Antonín Minařík, and Martin Humenik*

Self-assembly of a recombinant spider silk protein into nanofibrillar networks in combination with photolithography is used to produce diversely functionalized micropattern. Amino-modified substrates coated with a positive tone photoresist are processed into 1 μm deep arbitrarily shaped microwells, at the bottom of which spider silk proteins are covalently coupled to the deprotected aminated surface. The protein layer serves to seed the self-assembly of nanofibrils from the same protein in the microwells, forming immobilized few nanometers thin networks after the stripping of the photoresist. The nanofibrous micropattern can be functionalized by employing fluorescently modified spider silk variants during the self-assembly or by later covalent modification with nucleic acids. By repeating the photolithography and fibril assembly procedures, two functionally different and spatially defined pattern are created.

1. Introduction

The use of microstructured substrates is well established in the fields of biotechnology and bioanalytics.[1–3] These range from RNA microarrays, serving as high throughput arrays to screen gene expression,[4] to labs and organs on chips,[5,6] which are conveniently sized microfluidic implements used for conducting reactions,[7] analyzing substrate components[8,9] as well as cell–cell and cell–ligand interactions.[10,11] Due to their reduced size and compact construction, these require fewer resources for their production, reducing their costs, whilst also minimizing the amount of analyte. This enables a much higher throughput of samples and their readouts than with more conventional macroscopic methods.[10,12]

Photolithography represents a commonly used approach for microstructuring, whereby substrates are covered by a photosensitive resin, onto which illumination with a specific pattern imparts spatially defined soluble/insoluble areas, thus enabling selective deprotection of the surface and subsequent modifications at microscales.[10,13] Nonetheless, such microstructuring is often limited to the usage of covalently coupled synthetic polymers, due to the relatively harsh conditions involved in the photoresist processing.

Milder methods have been developed, such as polymer grafting using photocatalyzed coupling reactions,[14,15] but 3D structuring and additional functionalization of the networks require ever more complex polymers increasing associated synthesis costs. The polymerization of dopamine could also be used to generate a pattern with high fidelity, which can be further modified,[16,17] but the spectrum of reactions that can be employed, is limited to the dopamine moiety, requiring elaborate chemistry if desiring to spatiotemporally implement several different functions.

An approach to multilayering different functional substrates is presented by self-assembling protein films, which adhere to the prior layer using non-covalent interactions.[18] Such approaches are more versatile in the functionality and modification alternatives, but the introduction of specific functions on different spots of the substrate is often problematic. The non-covalent bonding, which predominates among the film layers, must also be resilient to breaking, limiting the variety of available interactions dependent on the application conditions, and impeding the development of a generally applicable system.

A strong non-covalent bonding interaction is found in silks, where the intrinsically random coil domains self-assemble into β-sheet-rich formations, whereby they are stabilized in a network of the same proteins.[19] The difference in solubility and the inducible nature of the conversion could be used for micropatterning.[20–24] Yet, a method, which provides the duality of being able to introduce high fidelity, high-resolution micropattern with a plethora of possible functionalization

Z. Lamberger,[+] M. Humenik
Department of Biomaterials
Faculty of Engineering Science
Universität Bayreuth
Prof.-Rüdiger-Bormann-Str. 1, 95447 Bayreuth, Germany
E-mail: martin.humenik@bm.uni-bayreuth.de

K. Kocourková, A. Minařík
Department of Physics and Materials Engineering
Faculty of Technology
Tomas Bata University in Zlín
Vavrečkova 275, Zlín 760 01, Czech Republic

K. Kocourková, A. Minařík
Centre of Polymer Systems
Tomas Bata University in Zlín
Třída Tomáše Bati 5678, Zlín 76001, Czech Republic

ⓘ The ORCID identification number(s) for the author(s) of this article can be found under https://doi.org/10.1002/admi.202201173.

[+]Present addresses: Department of Functional Materials in Medicine and Dentistry, University of Würzburg, Pleicherwall 2, 97070 Würzburg, Germany

ADVANCED
SCIENCE NEWS
www.advancedsciencenews.com

ADVANCED
MATERIALS
INTERFACES
www.advmatinterfaces.de

alternatives, as for instance two functionally and shapely distinct pattern introduced in proximity, has to be developed.

For this purpose, recombinant spider silk proteins can be employed. These were established as resilient and biocompatible materials[25,26] capable of controllable self-assembly into different morphologies.[27] Among these, nanofibrils were demonstrated to self-assemble in solutions or onto surfaces in a mild aqueous environment at low protein and phosphate concentrations.[28–30] Using chemically modified surfaces with the protein[31] or ultrathin nanofilms thereof,[32] the spider silk nanofibrils assembled on top into immobilized physically crosslinked networks, which displayed swelling and softening in the water, that is, properties similar to the bulk spider silk hydrogels.[33,34] The nanofibrillar nature of these nanohydrogels enabled a higher modification density and greater substrate accessibility compared to monolayers, whilst the mild aqueous self-assembly conditions in combination with the mechanical and chemical robustness of the nanohydrogels provided excellent scaffolds for embedding sensitive components such as enzymes and aptamers.[32] Spider silk proteins could be modified using both chemical[32,35] and genetic methods.[36–38] A plethora of possible functionalization alternatives, including enzymes, peptide tags, or nucleic acids, make the recombinant spider silk protein a promising scaffold for surface modifications suitable for a wide variety of biotechnological and bioanalytical applications.[39,40] If combined with the ability to microstructure the scaffolds into arbitrary shapes at microscale sizes, the applications thereof would be expandable into microtechnological fields with potential uses for instance in protein microarrays,[41] microstructured enzymatic arrays,[42] microfluidic chips used for substance analysis,[43] and microscale cell–cell or cell–material interaction assaying platforms.[44,45]

Herein, the self-assembling spider silk nanofibrils were explored in a combination with positive tone photolithography to produce functionalized microscale pattern of arbitrary shapes. The assembled nanofibrillar networks withstood even repetitive processing of the photoresist, thus enabling spatiotemporal patterning of the specifically codified protein microareas on one substrate with high position fidelity (**Figure 1**). Moreover, the fibrillar pattern was modified either by directly employing the self-assembly of modified protein variants or by using different coupling reactions after the self-assembly, revealing the versatility of the presented system to implement functionalization into the microstructures.

2. Results and Discussion

2.1. Generation of Microwells for Position-Specific Surface Modifications

APTES-modified glass substrates were used for the position-specific micropatterning of spider silk nanofibrillar networks. The micropattern was generated by spin coating of the substrates with a positive tone photoresist and selectively illuminating these with an arbitrary pattern (Figure 1 and Figure S1, Supporting Information), which generated microwells within the exposed areas after the development of the resin, hence, enabling spatially defined deprotection of the amino-modified glass surface.

A protein layer in the microwells could be created by adsorption to the surface. The adsorption of the fluorescein-labeled spider silk protein Flu-eADF4(C16)[28] was used to establish the processing parameters. Although the negatively charged protein (pI 3.7, due to the single charged amino acid residue E in the respective module) preferentially adsorbed to the microwell bottom furnished with amines, which are typically positively charged at the reaction pH of 7.1 (pKa of Lys-NH$_3^+$ app. 9.5), only negligible protein amounts retained after photoresist removal, likely due to the harsh conditions interfering with the non-covalent protein-to-surface bonding. To circumvent this, N-(3-dimethylaminopropyl)-N'-ethylcarbodiimide (EDC)-mediated covalent coupling of the glutamate residues in the spider silk protein to the primary amino moiety on the glass substrate was implemented, thus substantially improving the stability of the protein base layer, making it resilient to the photoresist removal process (**Figure 2**).

2.2. Position-Specific Self-Assembly

The coupled eADF4(C16) protein layer served as a seeding surface on which nanofibrillar networks could self-assemble. Fluorescein-modified Flu-eADF4(C16) was used to visualize the amount of assembled protein. As we described previously, the low phosphate concentrations trigger a structural transformation of the intrinsically unstructured spider silk monomers in solution into β-sheet-rich structures, resulting in a nucleation process and formation of cross-β-fibrils.[28,30,35,46] In case the protein is exposed on a surface, the nucleation and fibril growth occurred predominantly on the substrate instead of the solution.[31,32] We employed this principle to drive the self-assembly into the microwells. The specificity of the assembly was dependent on the protein concentration as shown in Figure S2, Supporting Information. The spider silk protein at a 5 µm concentration was asserted to have the best ratio between specific and unspecific self-assembly in the microwells, since the lower concentrations, despite being specific, resulted in little assembled protein in the pattern, whilst higher concentrations resulted in unspecific self-assembly on the photoresist surface (Figure S2D,E, Supporting Information), which hindered proper stripping of the resist afterward.

The microwells and the assembled material therein were characterized using profilometry and atomic force microscopy (AFM). The photoresist-based microwells displayed heights between 0.8 and 1.1 µm (**Figure 3**A,B and Figure S3, Supporting Information). As the surface roughness varied locally in dimensions of ≈40 nm (Figure 3C), likely due to contractions and microbubbles, which result from the photoresist hardening steps, that is, the processes of deep UV hardening and hard bake. Hence the comparatively small changes in the microwell's depth upon the protein assembly could not be determined before the photoresist stripping. Nonetheless, the surface topography in the differently treated microwells could be scanned and compared. The surface of the covalently coupled eADF4(C16) layer was mostly amorphous and smooth (Figure 3D). After the self-assembly from 2.5, 5, and 10 µm eADF4(C16) solutions (Figure 3E–G) the amount of nanofibrillar structures apparently increased, as well as the
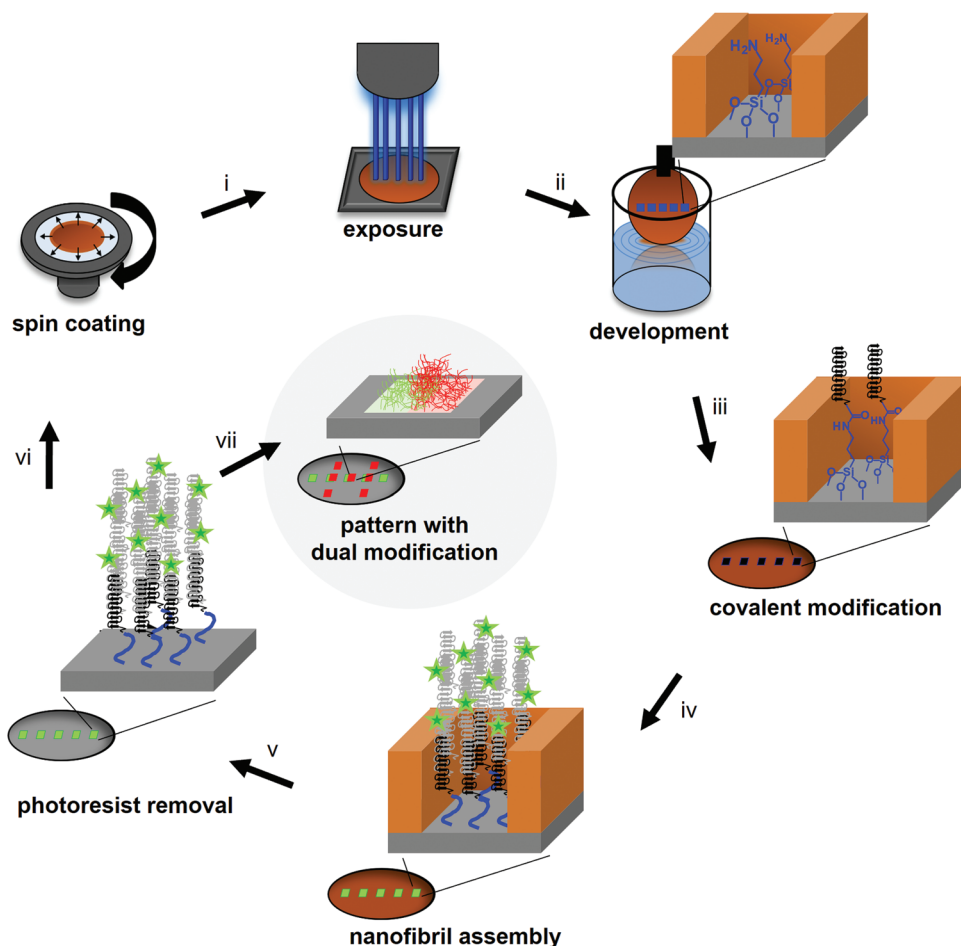
Figure 1. Schematic representation of procedures involved in the preparation of spider silk nanofibrillar micropattern. The process starts with the spin coating of a positive tone photoresist onto a glass substrate, followed by the illumination with the pattern using a maskless photolithography device (i) and subsequent selective removal of the soluble illuminated areas (ii), which leads to the formation of microwells with a chemically accessible bottom (blue structure). The exposed amine-modified glass surface is covalently coupled with the recombinant spider silk protein eADF4(C16) (black structure) (iii) serving as a nucleation layer upon which nanofibrils of a modified eADF4(C16) can be self-assembled (grey structure with green stars,) (iv). This is followed by the photoresist removal (v), which liberates the first fibrillar pattern (green). If desired (vi) the processing steps (i–v) can be repeated using a different illumination pattern and a differently modified variant of eADF4(C16) resulting in a dually patterned substrate (vii). These steps, when repeated twice with the use of fluorescein (Flu) and rhodamine (Rhod) labeled spider silk proteins, Flu-eADF4(C16) in the first cycle and Rhod-eADF4(C16) in the second cycle, enabled the production of two distinct spatiotemporally defined micropattern.

corresponding roughness of the surfaces, whilst the 10 µм sample revealed a denser spongiform-like surface.

As the limitation in the employed self-assembly concentration (Figure S2, Supporting Information) could pose an impediment to controlling the amount of self-assembled protein, we tested whether two consecutive rounds of self-assembly would circumvent this obstacle. The repetitive assembly at 5 µм Flu-eADF4(C16) yielded ≈40% increase in fluorescence signal (**Figure 4**A,B and Figure S4A, Supporting Information) compared to single self-assembly, whilst still retaining the specificity and fidelity of the micropattern after photoresist stripping. Alongside the capability of attaining greater heights of the nanofibrillar network and increased modification capacity, the consecutive assembly would also allow for the layering of distinctly modified networks atop each other.

The protein microstructures obtained after the photoresist stripping process were also analyzed with AFM and displayed

a similar topography as before the stripping (Figure 4C,D). The rougher surface of the fibrillar networks could clearly be distinguished from the smooth surrounding glass surface (Figure 4C). Depending on the self-assembly concentrations and number of consecutive assemblies, the heights of the assembled protein material in the dry state varied from 5–20 nm (Figure 4D,E). The microstructures could have an arbitrary shape and size ranging from the smallest tested pattern with a width of 50 µm (Figure S4B, Supporting Information), which was approaching the resolution limit of the employed photolithography device. A size limitation on the higher end was not reached, as 200–250 µm wide pattern were still easily producible. The length could also be arbitrarily varied ranging from 50 µm up to several mm, with no apparent length limitation (Figure 4A,B and Figure S2B, Supporting Information). The micropatterned fibrillar networks were similarly resilient as the nonpatterned nanohydrogels[32] and could be stored in
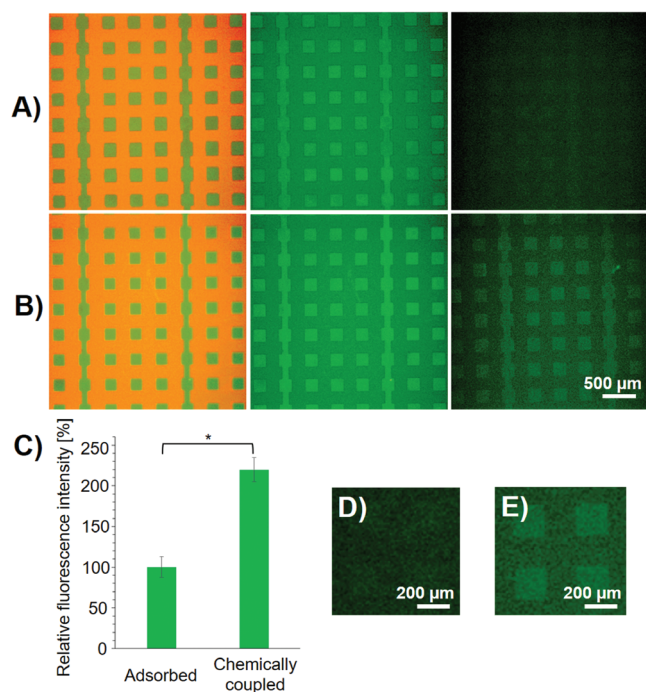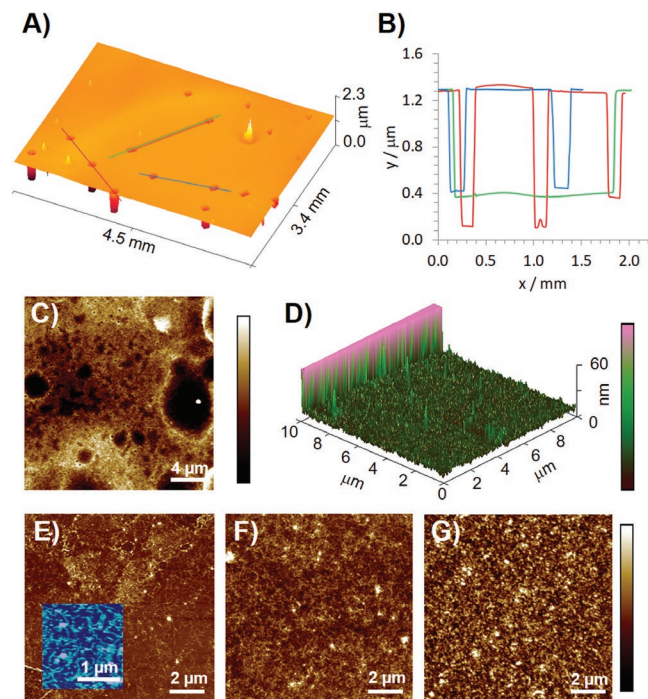
Figure 2. Comparison of protein layer retention with and without covalent coupling. Fluorescence microscopic images of Flu-eADF4(C16) in microwells either adsorbed in (A) or covalently coupled to the amino-modified surface in (B). The fluorescent images in (A) and (B) showing microwells using the red photoresist (left) and green fluorescein (left and middle panel) fluorescence, as well as the surface after photoresist removal (right). Relative fluorescence intensities of the micropattern from (A) and (B) (right panels) were compared in (C), whereas details of the microstructures are shown in (D) and (E), respectively. Plotted values presented as mean ± fluorescence intensity, $n = 3$, and p-values were calculated using a one-way ANOVA, $*p < 0.05$. Scale bars 500 μm in (A) and (B), 200 μm in (D) and (E).


Figure 3. Characterization of the spider silk self-assembly in microwells. A) Optical profilometry image of microwells in the photoresist. B) Cross sections of the microwells in (A) as determined by optical profilometry. C) AFM scan of the photoresist surface. D) Topography of the chemically coupled eADF4(C16) in the microwell as analyzed with AFM. E,F) Surfaces of the fibrillar networks assembled from 2.5, 5, and 10 μM protein, respectively. Inset in (E) represents a focused scan of the fibrillar surface. Color bars: 0–40 nm in (C), 0–60 nm in (D), and 0–20 nm in (E–G).

a dry state at 4 °C for at least a month without any apparent changes to the structures.

The photoresist served as a border to spatially limit the self-assembly, only enabling the fibrils to grow in height in the predetermined microwells, instead of assembling in all directions, which would otherwise result in a loss of resolution and shape fidelity. Hence the photolithographic approach with the photoresist being present during the self-assembly is essential and offers a distinct advantage over other conventionally used methods, such as micro spotting, since it enables the production of much higher stable fibrous pattern, with high fidelity, resolution, and arbitrary shape, whilst also conveniently conducting the assembly for all desired microwells at once. If a very diverse array of functions would be desired, the defined assembled fibrillar scaffolds may then be further functionalized using micro spotting of reactive mixtures, upholding the scaffolds' shape fidelity, whilst specifically modifying its fibrils.

The modification of the fibrillar micropattern with DNA had been tested and enabled further functionalization of the pattern. The pattern made by assembling N₃-eADF4(C16) (azido modification on the protein N-terminus)[32] were modified either site-specifically with DBCO-DNA in a strain promoted cycloaddition after the photoresist stripping or in an EDC facilitated

coupling of H₂N-modified DNA (targeting Glu residues in the protein sequence) in the microwells and subsequent stripping. The coupled single-stranded DNA strands (ssDNA) could be detected by a complementary fluorescent probe (Figure S5A,B, Supporting Information) showing that the micropattern was susceptible to biofunctionalization before, as well as after the photoresist removal. Moreover, not only the fibrillar networks were stable enough to withstand the photoresist stripping, but also the coupled ssDNA (Figure S5B, Supporting Information), likely due to the relatively short exposure to the basic stripping conditions in the diluted developer solution.

2.3. Dual Patterning of Fibrillar Networks

The recombinant spider silk protein forms cross-β nanofibrils, which were shown to remain unaffected by denaturing conditions such as high temperatures or 8 M urea.[35,46] Interestingly, the fibrillar networks made thereof, which are crosslinked just by physical interaction,[32] showed good resilience in the microstructures during the harsh photoresist stripping, including an alkaline developer solution (pH 13) and organic solvents such as acetone and ethyl acetate. Such harsh conditions would likely denature and/or remove a majority of polymeric or proteinaceous networks if no covalent crosslinking would be employed. The successful stripping indicated that the
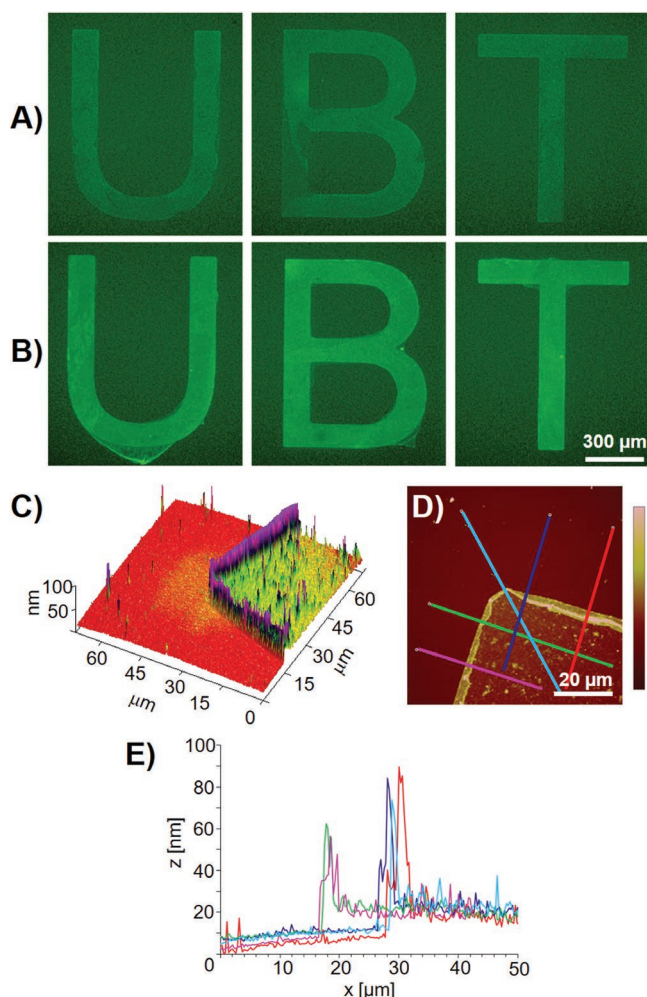
Figure 4. Analysis of protein micropattern after photoresist removal. Fluorescence images of microstructures after the photoresist stripping are presented, after A) one round and B) two rounds of the self-assembly (5 μM Flu-eADF4(C16) in 100 mM phosphate buffer for 16 h and washes in between each round). C) 3D representation of the AFM height scan on the "T" microstructure edge in (B). D) The plain representation of the AFM scan in (C) with the marking of the cross sections as evaluated in (E). Color bar 0–101 nm in (D). Scale bar 500 μm in (A) and (B), 20 μm in (D).

patterned proteins could potentially withstand several rounds of the photoresist spin coating and stripping. The creation of a differently labeled protein pattern in the next cycle would allow the positioning of distinctly functionalized and arbitrarily shaped protein microstructures on the same substrate. Hence, two cycles of photolithography, self-assembly, and photoresist stripping were conducted. In the first cycle, 5 μM unmodified eADF4(C16) in the chemical coupling step and consecutively 2.5 μM Flu-eADF4(C16) in the self-assembly steps were employed, whilst in the second round, Rhod-eADF4(C16) was used in the fibrilization instead at the same experimental conditions. Surprisingly, despite having been covered by the photoresist, the protein fibrillar layers from the first pattering cycle retained their shape fidelity and integrity. Using the same substrate, two distinct pattern could be set on the surface either far apart, in proximity, or even overlapping (**Figure 5**). This clearly demonstrated the spatiotemporal control over the
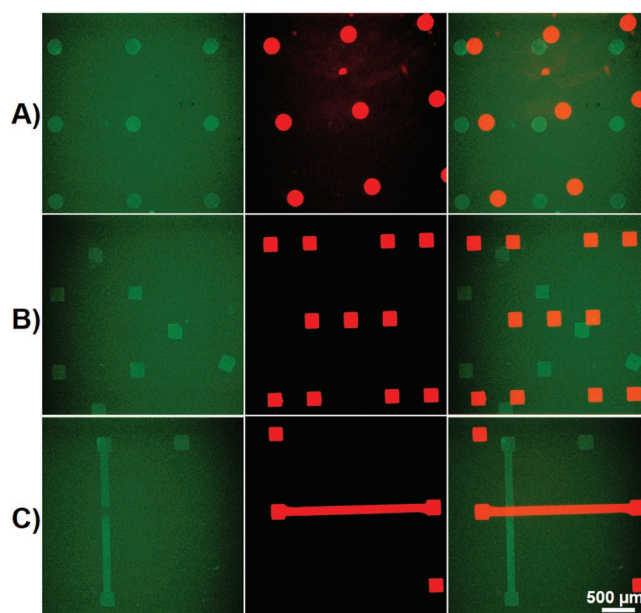
Figure 5. Dually patterned fibrillar networks. Fluorescence images of sequentially patterned Flu-eADF4(C16) (left panels) and Rhod-eADF4(C16) (middle) and the merged images (right); in (A–C). Scale bar 500 μm in (A–C).

position of distinctly functionalized fibrillar networks on the substrates.

Sequentially patterned protein microstructures, as exemplarily shown in Figure 5, were also analyzed using AFM, whereby those assembled in the first and in the second patterning round showed similar heights (**Figure 6**A,B, green and blue lines) indicating minimal losses of the assembled material after each cycle. Interestingly, in the overlapping locations, the pattern height was cumulative (Figure 6B, red and violet line), confirming positioning fidelity and robustness of the assembly
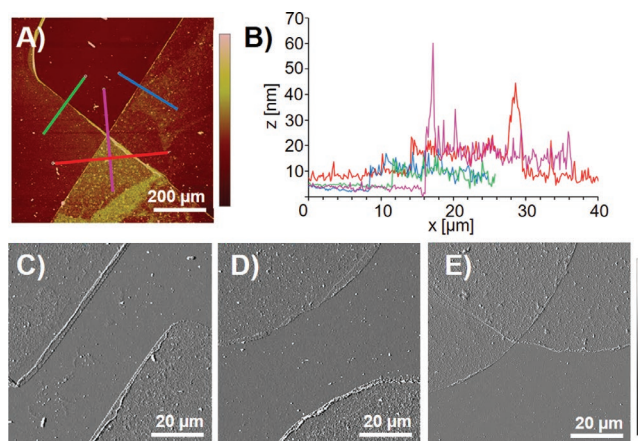
Figure 6. AFM analysis of dual protein patterning. A) AFM height scan of the overlapping Flu-eADF4(C16) and Rhod-eADF4(C16) cross micropattern as seen in Figure 5C (bottom right corner) inclusive colored lines representing evaluated cross sections in (B). AFM amplitude scans showing proximal in (C) and (D) and overlapping in (E) dual patterned fibrillar networks. Color bars 0–59 nm (B) and −18 to 18 mV (D–F). Scale bar 200 μm in (A) and 20 μm (C–E).

process. Further examples of distinctly placed microstructures as obtained after the dual patterning procedure in Figure 5 are demonstrated in Figure 6C–E.

Since the pattern showed no changes in height and shape after each photolithography round, the number of the procedure repetitions can likely be increased in the future to prepare multicomponent arrays. The upper limit has not been explored yet but is likely limited by the ability of various modifications covalently incorporated in the spider silk microstructures to retain their functions after the repeating photoresist processing.

3. Summary

The robust properties of the fibrillar networks composed of recombinant spider silk proteins enabled the combination of the protein self-assembly with the harsh photolithography processes such as photoresist spin coating and stripping. Thus, arbitrarily shaped microwells could be created in a positive tone resist atop of the amino-modified glass surface, hence defining the positions available for the covalent coupling of an eADF4(C16) layer allowing further immobilization of fibrillar networks upon nucleation of the same protein in the wells. The preparation of the microscale protein arrays was also employed in the sequential photopatterning and self-assembly procedures revealing the capability of the developed system to produce dissimilarly functionalized protein microstructures at adjustable proximity. Considering the broad variability of available spider silk protein genetical variants[38,47–49] and chemical[32,35] modifications, such a system will offer many alternatives for screening and comparing different surface modifications under the same conditions at a microscale resolution and with variable spacing in-between the different material and shapes based on the protein microstructures. Such variable setup could be used in the future, for instance, in studies of material-cell interactions[44,45] at the concomitant influence of microstructure shapes and/or co-culturing of different cell lines specifically attracted by employed adhesion tags on the eADF4(C16) scaffolds to study the influence of biological signals on cell behavior. In further developments of the presented system, spatially selective implementation of enzymatic functionalities into the pattern would be possible in post-lithography processing using addressable hybridization between the DNA-modified micropattern and complementary DNA-modified protein chimeras, protein binding DNA-aptamers,[32,50] or protein binding tags.[51,52] This would enable spatiotemporal implementation of different enzymes in micro-analytical devices, growth factors in tissue engineering, or cancer markers in diagnosis and therapy. Moreover, the established methods using glass substrates would also enable glass-to-polydimethylsiloxane (PDMS) bonding suitable for the implementation of microfluidic chips.[53,54] On the other side, the presented self-assembly of the spider silk protein and modified variants thereof enable employing mild aqueous conditions. The formation of corresponding fibrillar networks has been shown to leave unchanged tertiary structures of fused protein modifications or secondary structures of coupled nucleic acids.[32,38] Thus, further attempts, which include mild water-soluble photoresists and/or protective sacrificial polymer layers,[55] could lead to the development of fully biocompatible

photolithography. Hence, the pattern of environmentally sensitive proteins will be possible in the spider silk nanofibrillar networks, which increase the surface area due to accommodation of the modification along the fibrils, whilst also providing a protective nanohydrogel-like environment.[32]

4. Experimental Section

Materials: If not stated otherwise, all chemicals were supplied by Merck KGaA (Germany) in analytical grade. Recombinant spider silk protein eADF4(C16) (sequence: (MASMTGGQQMGRGSM(GSSAA AAAAAASGPGGYGPENQGPSGPGGYGPGGP)₁₆G) was prepared as published.[56] The rhodamine- and fluorescein-modified variants Flu- and Rhod-eADF4(C16) were produced by coupling eADF4(C16) with *N*-hydroxysuccinimidester (NHS)-Rhodamine (Thermo Fisher Scientific) or NHS-Fluorescein (Thermo Fisher Scientific) as described in Ref. [28]. Ultrapure water in the experiments was obtained using a Millipore system (Merck KGaA).

Photolithographic Preparation of Microwells: Glass coverslips (∅19 mm) were cleaned using acetone, isopropanol, and Radio Corporation of America (RCA) cleaning procedure (developed by Werner Kern at RCA laboratories in the late 1960s),[57] before activation with 100% O_2-plasma at 0.2 mbar for 1 min and a silanization using 0.1% v/v APTES in ethanol for 16 h.[58] The amino-activated slides were pre-baked at 120 °C for 10 min on a precision hot plate HP 60 (Torrey Pines Scientific, Inc., USA) to evaporate adsorbed H_2O. Afterward, the coverslips were placed onto a spin coater and 55 µL of Ti-Prime (Microchemicals GmbH, Germany) were applied at 50 rps for 30 s with an acceleration time of 3 s. The coated plates were incubated for 2 min at 120 °C on the hotplate and spin coated with 55 µL of the AZ 1512 HS positive photoresist (Microchemicals GmbH, Germany) resulting in a photoresist thickness of ≈1 µm. The coverslips were post-baked at 100 °C for 2 min and subsequently illuminated using SmartPrint maskless lithography equipment based on a µLCD projection technology (Microlight3D) at 435 nm (10.2 mW cm⁻²) for 40 s. The microwells were developed in 1:4 v/v AZ 400 K Developer (Microchemicals GmbH, Germany)/H_2O mixture using agitation for 30 s. To render the microstructures more resilient against longer incubations in aqueous media, hardening was conducted using exposure to a deep UV light (Benda NU-6 KL UV lamp) for 2.5 min followed by a hard bake at 130 °C for 5 min.

Assembly of Fibrillar Networks in Microwells: Aqueous protein solutions were prepared by dissolution in 6 M guanidinium thiocyanate and dialyzed as described[35] into 50 mM Na salt of *N*-(2-hydroxyethyl) piperazine-*N*′-(2-ethanesulfonic acid) (HEPES-Na) pH 7.1 buffer. The protein solution was centrifuged at 55 000 rpm (centrifuge Optima MAX-XP, rotor TLA-55, Beckman Coulter Inc., USA) at 4 °C for 55 min, with the supernatant being used for further processes.

After the photolithography, the amino-modified surface in the deprotected microwells was covalently modified in a solution of 2.5 µM eADF4(C16) and 2.5 mg mL⁻¹ *N*-(3-dimethylaminopropyl)-*N*′-ethylcarbodiimide-hydrochloride (EDC) in 50 mM HEPES-Na, pH 7.1 for 16 h. Thereafter, the coverslips were washed with 50 mM HEPES-Na pH 7.1 and incubated in a solution of 5 µM eADF4(C16) or one of its chemically modified variants in 100 mM K-Pi, 50 mM HEPES-Na pH 7.1 for 16 h. The coverslips were washed with 10 mM Tris/HCl 100 mM NaCl and subsequently Milli-Q H_2O.

Photoresist Stripping: The photoresist was stripped using a bright field lamp (Makita DEADML801) at the maximum intensity for 2 min followed by 10 min incubations in solutions of 1:4 v/v AZ 400 K Developer/H_2O, 2:1 v/v acetone/ethyl acetate, acetone and Milli-Q H_2O.

Dual Patterning: After the stripping procedure, the substrates modified with one type of the fibrillar networks were pre-baked at 120 °C for 5 min and spin coated with 55 µL of the AZ 1512 HS positive photoresist (Microchemicals GmbH, Germany), followed by the previously described hardening, illumination and microwell development, assembly of the second protein assembly, and photoresist stripping procedures.

Atomic Force Microscopy: AFM scanning of dry samples was performed on a Dimension ICON with Nanoscope V controller in TappingMode using Si cantilevers (OTESPA-R3, a resonance frequency of 300 kHz, spring constant of 26 N m^{-1}; Bruker, USA). Data were processed using Nanoscope Analysis 1.8 (Bruker, USA).

Surface Profilometry: The surface topography of the microwells was characterized by a noncontact profilometer Nano Contour model GT-K (Bruker). The samples were measured using white light and a lens with a magnification of 2.5×. Images were processed using Gwyddion 2.59 software.

Statistical Analysis: If not indicated otherwise, the experimental data were evaluated using the arithmetic mean and standard deviation of triplicates. Comparison of multiple sample groups was statistically assessed using a one-way ANOVA test in the software Excel (Microsoft Corporation, USA), using the data analysis function. Data were considered as statistically significant if $p \leq 0.05$.

Supporting Information

Supporting Information is available from the Wiley Online Library or from the author.

Conflict of Interest

The authors declare no conflict of interest.

Author Contributions

The manuscript was written through the contributions of all authors. All authors have given approval to the final version of the manuscript.

Data Availability Statement

The data that support the findings of this study are available from the corresponding author upon reasonable request.

[1] C. Wiles, P. Watts, S. J. Haswell, E. Pombo-Villar, *Lab Chip* **2001**, *1*, 100.
[2] F. Qian, M. Baum, Q. Gu, D. E. Morse, *Lab Chip* **2009**, *9*, 3076.
[3] R. D. Chambers, D. Holling, R. C. Spink, G. Sandford, *Lab Chip* **2001**, *1*, 132.
[4] S. C. Sealfon, T. T. Chu, *Methods Mol. Biol.* **2011**, *671*, 3.
[5] L. A. Low, C. Mummery, B. R. Berridge, C. P. Austin, D. A. Tagle, *Nat. Rev. Drug Discovery* **2021**, *20*, 345.
[6] J. Dornhof, J. Kieninger, H. Muralidharan, J. Maurer, G. A. Urban, A. Weltin, *Lab Chip* **2021**, *22*, 225.
[7] M. Matlosz, W. Ehrfeld, in *Microreaction Technology* (Eds: J.P. Baselt), Springer, Berlin, Heidelberg **2001**.
[8] H.-C. Lai, C.-H. Wang, T.-M. Liou, G.-B. Lee, *Lab Chip* **2014**, *14*, 2002.
[9] K. Kikkeri, D. Wu, J. Voldman, *Lab Chip* **2021**, *22*, 100.
[10] O. J. Scheideler, C. Yang, M. Kozminsky, K. I. Mosher, R. Falcón-Banchs, E. C. Ciminelli, A. W. Bremer, S. A. Chern, D. V. Schaffer, L. L. Sohn, *Sci. Adv.* **2020**, *6*, eaay5696.
[11] L. Huang, X. Zhang, Y. Feng, F. Liang, W. Wang, *Lab Chip* **2021**, *22*, 1206.
[12] E. W. K. Young, D. J. Beebe, *Chem. Soc. Rev.* **2010**, *39*, 1036.
[13] C. Luo, C. Xu, L. Lv, H. Li, X. Huang, W. Liu, *RSC Adv.* **2020**, *10*, 8385.
[14] M. Steenackers, A. Küller, S. Stoycheva, M. Grunze, R. Jordan, *Langmuir* **2009**, *25*, 2225.
[15] T. B. Stachowiak, F. Svec, J. M. J. Fréchet, *Chem. Mater.* **2006**, *18*, 5950.
[16] I. Topolniak, A. M. Elert, X. Knigge, G. C. Ciftci, J. Radnik, H. Sturm, *Adv. Mater.* **2022**, *34*, 2109509.
[17] X. Du, L. Li, J. Li, C. Yang, N. Frenkel, A. Welle, S. Heissler, A. Nefedov, M. Grunze, P. A. Levkin, *Adv. Mater.* **2014**, *26*, 8029.
[18] D. Xu, S. M. Bartelt, S. Rasoulinejad, F. Chen, S. V. Wegner, *Mater. Horiz.* **2019**, *6*, 1222.
[19] C. Dicko, D. Knight, J. M. Kenney, F. Vollrath, *Int. J. Biol. Macromol.* **2005**, *36*, 215.
[20] H. Perry, A. Gopinath, D. L. Kaplan, L. Dal Negro, F. G. Omenetto, *Adv. Mater.* **2008**, *20*, 3070.
[21] Y. H. Youn, S. Pradhan, L. P. da Silva, I. K. Kwon, S. C. Kundu, R. L. Reis, V. K. Yadavalli, V. M. Correlo, *ACS Biomater. Sci. Eng.* **2021**, *7*, 2466.
[22] N. E. Kurland, J. Kundu, S. Pal, S. C. Kundu, V. K. Yadavalli, *Soft Matter* **2012**, *8*, 4952.
[23] N. E. Kurland, T. Dey, S. C. Kundu, V. K. Yadavalli, *Adv. Mater.* **2013**, *25*, 6207.
[24] B. G. Kumar, R. Melikov, M. M. Aria, A. U. Yalcin, E. Begar, S. Sadeghi, K. Guven, S. Nizamoglu, *ACS Biomater. Sci. Eng.* **2018**, *4*, 1463.
[25] T. Scheibel, *Microb. Cell Fact.* **2004**, *3*, 14.
[26] C. Vendrely, T. Scheibel, *Macromol. Biosci.* **2007**, *7*, 401.
[27] M. Humenik, A. M. Smith, T. Scheibel, *Polymers* **2011**, *3*, 640.
[28] M. Humenik, A. M. Smith, S. Arndt, T. Scheibel, *J. Struct. Biol.* **2015**, *191*, 130.
[29] M. Humenik, G. Lang, T. Scheibel, *Nanomed. Nanobiotechnol.* **2018**, *10*, e1509.
[30] M. Humenik, M. Magdeburg, T. Scheibel, *J. Struct. Biol.* **2014**, *186*, 431.
[31] A. Molina, T. Scheibel, M. Humenik, *Biomacromolecules* **2019**, *20*, 347.
[32] M. Humenik, T. Preiß, S. Gödrich, G. Papastavrou, T. Scheibel, *Mater. Today Bio* **2020**, *6*, 100045.
[33] K. Schacht, T. Scheibel, *Biomacromolecules* **2011**, *12*, 2488.
[34] A. Lechner, V. T. Trossmann, T. Scheibel, *Macromol. Biosci.* **2021**, *22*, 2100390.
[35] M. Humenik, T. Scheibel, *ACS Nano* **2014**, *8*, 1342.
[36] S. Kumari, G. Lang, E. DeSimone, C. Spengler, V. T. Trossmann, S. Lücker, M. Hudel, K. Jacobs, N. Krämer, T. Scheibel, *Mater. Today* **2020**, *41*, 21.

[37] J. Petzold, T. B. Aigner, F. Touska, K. Zimmermann, T. Scheibel, F. B. Engel, *Adv. Funct. Mater.* **2017**, *27*, 1701427.

[38] M. Humenik, M. Mohrand, T. Scheibel, *Bioconjugate Chem.* **2018**, *29*, 898.

[39] M. Koenig, U. König, K.-J. Eichhorn, M. Müller, M. Stamm, P. Uhlmann, *Front. Chem.* **2019**, *7*, 101.

[40] A. E. M. Wammes, M. J. E. Fischer, N. J. de Mol, M. B. van Eldijk, F. P. J. T. Rutjes, J. C. M. van Hest, F. L. van Delft, *Lab Chip* **2013**, *13*, 1863.

[41] D. A. Hall, J. Ptacek, M. Snyder, *Mech. Ageing Dev.* **2007**, *128*, 161.

[42] J. Yan, V. A. Pedrosa, A. L. Simonian, A. Revzin, *ACS Appl. Mater. Interfaces* **2010**, *2*, 748.

[43] P. Cui, S. Wang, *J. Pharm. Anal.* **2019**, *9*, 238.

[44] C. Heinritz, Z. Lamberger, K. Kocourková, A. Minařík, M. Humenik, *ACS Nano* **2022**, *16*, 7626.

[45] Z. Lamberger, H. Bargel, M. Humenik, *Adv. Funct. Mater.* **2022**, https://doi.org/10.1002/adfm.202207270.

[46] M. Humenik, M. Drechsler, T. Scheibel, *Nano Lett.* **2014**, *14*, 3999.

[47] M. B. Elsner, H. M. Herold, S. Müller-Herrmann, H. Bargel, T. Scheibel, *Biomater. Sci.* **2015**, *3*, 543.

[48] S. Wohlrab, K. Spieß, T. Scheibel, *J. Mater. Chem.* **2012**, *22*, 22050.

[49] T. U. Esser, V. T. Trossmann, S. Lentz, F. B. Engel, T. Scheibel, *Mater. Today Bio.* **2021**, *11*, 100114.

[50] H. Ma, J. Liu, M. M. Ali, M. A. I. Mahmood, L. Labanieh, M. Lu, S. M. Iqbal, Q. Zhang, W. Zhao, Y. Wan, *Chem. Soc. Rev.* **2015**, *44*, 1240.

[51] B. Zakeri, J. O. Fierer, E. Celik, E. C. Chittock, U. Schwarz-Linek, V. T. Moy, M. Howarth, *Proc. Natl. Acad. Sci. USA* **2012**, *109*, E690.

[52] T. G. M. Schmidt, A. Skerra, *Nat. Protoc.* **2007**, *2*, 1528.

[53] A. Sridhar, A. Kapoor, P. S. Kumar, M. Ponnuchamy, B. Sivasamy, D.-V. N. Vo, *Environ. Chem. Lett.* **2022**, *20*, 901.

[54] V. Narayanamurthy, Z. E. Jeroish, K. S. Bhuvaneshwari, P. Bayat, R. Premkumar, F. Samsuri, M. M. Yusoff, *RSC Adv.* **2020**, *10*, 11652.

[55] A. K. Grebenko, K. A. Motovilov, A. V. Bubis, A. G. Nasibulin, *Small* **2022**, *18*, 2200476.

[56] D. Huemmerich, C. W. Helsen, S. Quedzuweit, J. Oschmann, R. Rudolph, T. Scheibel, *Biochemistry* **2004**, *43*, 13604.

[57] W. Kern, *J. Electrochem. Soc.* **1990**, *137*, 1887.

[58] A. Miranda, L. Martínez, P. A. A. de Beule, *MethodsX* **2020**, *7*, 100931.